articles

Optical gain in silicon nanocrystals

L. Pavesi*, L. Dal Negro*, C. Mazzoleni*, G. Franzò† & F. Priolo†

* INFM & Dipartimento di Fisica, Università di Trento, Via Sommarive 14, 38050 Povo, Italy
† INFM & Dipartimento di Fisica e Astronomia, Università di Catania, Corso Italia 57, 95129 Catania, Italy

....

Adding optical functionality to a silicon microelectronic chip is one of the most challenging problems of materials research. Silicon is an indirect-bandgap semiconductor and so is an inefficient emitter of light. For this reason, integration of optically functional elements with silicon microelectronic circuitry has largely been achieved through the use of direct-bandgap compound semiconductors. For optoelectronic applications, the key device is the light source—a laser. Compound semiconductor lasers exploit low-dimensional electronic systems, such as quantum wells and quantum dots, as the active optical amplifying medium. Here we demonstrate that light amplification is possible using silicon itself, in the form of quantum dots dispersed in a silicon dioxide matrix. Net optical gain is seen in both waveguide and transmission configurations, with the material gain being of the same order as that of direct-bandgap quantum dots. We explain the observations using a model based on population inversion of radiative states associated with the Si/SiO$_2$ interface. These findings open a route to the fabrication of a silicon laser.
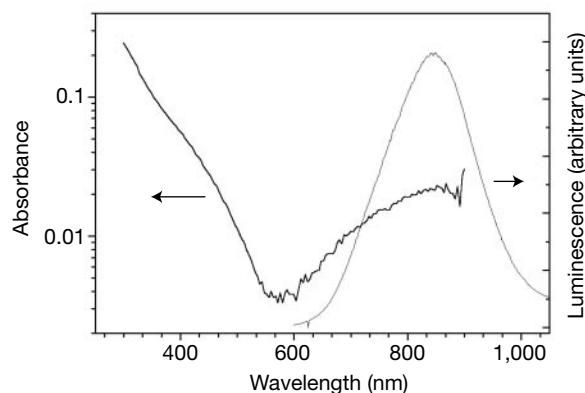
Silicon, the mainstay semiconductor in microelectronic circuitry, has been considered unsuitable for optoelectronic applications owing to its indirect electronic bandgap, which limits its efficiency as a light emitter. Recently, room-temperature light emission from silicon has been shown to be possible when the silicon is in the form of a low-dimensional system[1–5] or when selected active impurities (such as erbium[6]) and/or new phases (such as iron disilicide[7]) are inserted into the silicon lattice. All manner of low-dimensional silicon systems—such as porous silicon[1,2,5], silicon nanocrystals[3], silicon/insulator superlattices[4], silicon nano-pillars[8]—are being actively investigated as a means of improving the light-emission properties of silicon. The physical mechanism underlying high external quantum efficiencies for photoluminescence in low-dimensional silicon is mainly that of the quantum confinement of excitons in a nanometre-scale crystalline structure[9], although the silicon/dielectric interface is also thought to play an active role in both the passivation of non-radiative states and the formation of radiative states[10]. Such work has led to many claims of a future role for silicon in photonic applications[9,11–13], yet a silicon laser has remained unlikely[14].

To produce a silicon-based laser, we should demonstrate its light amplification or stimulated emission[15]. But light amplification in silicon is difficult because (1) it has efficient free carrier absorption, which reduces the net gain available for laser action[14]; (2) there is
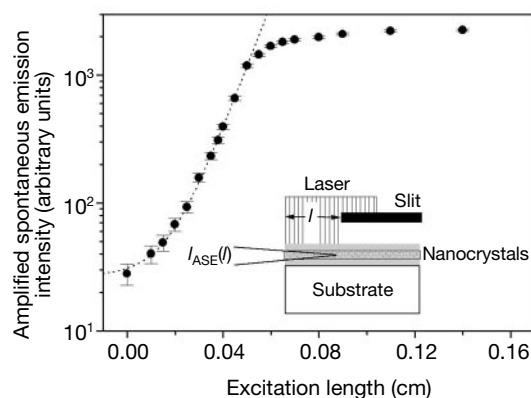
significant Auger saturation of the luminescence intensity at high power[9]; and (3) there is significant size-dependence of the radiative energies in Si nanostructures, which yields large inhomogeneous broadening and significant optical losses in the system[16]. Here we report measurements of stimulated emission and light amplification in Si nanostructures and demonstrate optical gain in a single pass configuration. Population inversion is realized between the fundamental and a radiative state associated with the nanocrystal–oxide interface[10]. These findings could lead the way to a silicon-based laser.

Silicon nanocrystals

Low-dimensional silicon nanocrystals have been produced by negative ion implantation (80 keV; 1×10^{17} Si ions cm^{-2}) into ultra-pure quartz substrates or into thermally grown silicon dioxide layers on Si substrates, followed by high-temperature thermal annealing (1,100 °C for 1 h). Quartz wafers (hereafter referred to as

Figure 2 Amplified spontaneous emission intensity (ASE, disks) versus excitation stripe length (l) of Si nanocrystals embedded in a quartz matrix. Recording wavelength, 800 nm. A fit to the data with equation (1) is shown as the dashed line. The inset shows the experimental method. A cylindrical lens was used to focus the laser beam on the sample surface on a stripe 10-μm wide and of variable length. Only the central part of the laterally unfocused laser spot was used to excite the sample. Measurements show that within these experimental conditions the laser power density on the sample surface is constant and independent of l. An optical 40 × objective imaged the sample edge on a 40-μm pinhole so that only the light coming from the near sample surface region was collected. The use of a pulsed laser avoided any thermal heating of the sample. The excitation conditions were 1 kW cm^{-2} mean power at a wavelength of 390 nm.

Figure 1 Room temperature absorbance and luminescence of Si nanocrystals embedded in a quartz matrix. The experimental set-up limited the absorbance measurement range. The absorbance of the quartz wafer was subtracted from the measured spectra. The 488 nm line of an Ar laser excited the luminescence.
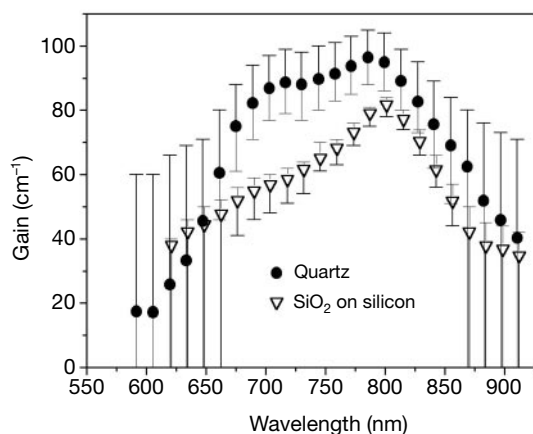
as 'sample A') were used for optical transmission experiments, and silicon wafers (hereafter referred to as 'sample B') to demonstrate microelectronics compatibility. Transmission electron microscopy of these samples showed silicon nanocrystals embedded within the oxide matrix. They were formed in a region centred at a depth of 110 nm from the sample surface and extending for a thickness of 100 nm; they were ~3 nm in diameter, with a concentration of 2×10^{19} cm^{-3}. If we consider the Maxwell–Garnett approximation, we can estimate an effective refractive index of 1.89 for the nanocrystal region (see Fig. 3 in the Supplementary Information). For nanocrystals produced by plasma-enhanced chemical vapour deposition (PE-CVD)[17], an effective refractive index of 1.71 was measured by ellipsometry. We note that in sample A, this causes the formation of a planar waveguide with an optical filling factor of about 9.7% when a refractive index of 1.89 is considered, or of 1.17% when a refractive index of 1.71 is assumed (see Fig. 3 in the Supplementary Information).

Absorbance and luminescence spectra at room temperature for sample A are shown in Fig. 1. A single wide emission band peaked at 800 nm, characteristic of the radiative recombination of carriers in Si nanocrystals, is observed. Absorbance measurements revealed a band in the near-infrared and a rising absorption edge at shorter wavelengths. The rising edge is due to absorption in the quantum confined states of the nanocrystals[18], whereas the peculiar feature of the near-infrared absorption band is caused by a Si=O interface state[10,19,20]. As predicted by theory[10,21] and inferred from experiment, the interface state is formed at the interface between the Si nanocrystals and the SiO$_2$ matrix. The microscopic nature of these interface states is still under debate[10,21]. Very good quality SiO$_2$ and Si nanocrystals are needed to observe this interface state, which in other Si-based systems is hindered by interfaces with defects or the low quality of the oxide. We note the spectral coincidence of the emission band and the interface state absorption band, suggesting that radiative emission in Si nanocrystals occurs through a radiative state associated with the nanocrystal–oxide interface. Time-resolved luminescence, under picosecond excitation, on our nanocrystals showed a very fast rise time, within our experimental sensitivity (some nanoseconds)[22]. The decay time of the luminescence was in the microsecond range; it is dependent on the emission energy[23].

Light amplification

To measure light amplification we used the variable strip length method (see the inset of Fig. 2)[24]. The sample is optically excited by a doubled Ti:sapphire laser beam ($\lambda = 390$ nm, 2-ps pulse width, 82-MHz repetition rate) in a stripe-like geometry with variable length (l). The amplified spontaneous emission intensity I_{ASE} that is emitted from the sample edge (observation angle $\phi = 0$) is measured as a function of l. From a fit of the resulting curve, the optical gain g can be deduced at every wavelength. By assuming a one-dimensional amplifier model, I_{ASE} can be related to g by[15,24]

$$I_{ASE}(l) \propto \frac{I_{SPONT} \times l}{g - \alpha}\left(e^{(g-\alpha)l} - 1\right) \quad (1)$$

where I_{SPONT} is the spontaneous emission intensity per unit length and α an overall loss coefficient. The gain measured in this way is the modal gain[15]. Figure 2 shows I_{ASE} versus l in Si nanocrystals measured at a wavelength of 800 nm. For small values of l (<0.05 cm), an exponential increase of I_{ASE} is observed that indicates the occurrence of amplified spontaneous emission. A fit with equation (1) yields the net modal gain $g - \alpha = 100 \pm 10$ cm^{-1}. For large values of l (>0.05 cm), I_{ASE} saturates as expected for any finite power supply amplification mechanism. At
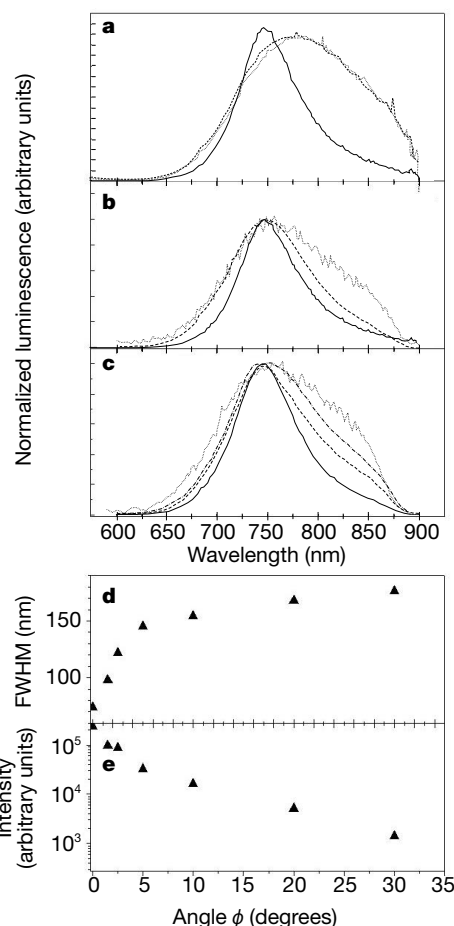
Figure 4 Amplified spontaneous emission spectra of sample A for different measurement conditions. **a**, Amplified spontaneous emission (ASE) spectra for a constant excitation length $l = 2,000$ μm and various power densities P: continuous line 2.3 kW cm^{-2}, dashed line 1 kW cm^{-2}, dotted line 170 W cm^{-2}. **b**, ASE spectra for constant $P = 2.3$ kW cm^{-2} and various l values: $l = 2,000$ μm continuous line, $l = 650$ μm dashed line, $l = 200$ μm dotted line. **c**, ASE spectra for constant $P = 1$ kW cm^{-2} and $l = 3,000$ μm and various observation angles ϕ. ϕ is defined with respect to the optical axis of the one-dimensional amplifier. Continuous line $\phi = 0°$, dashed line $\phi = 1.5°$, dash-dotted line $\phi = 2.5°$, dotted line $\phi = 20°$. The low energy cut-off of the photomultiplier used to record the data deforms the spectra for wavelength longer than 880 nm. **d**, Full-width at half-maximum (FWHM) of the ASE emission as a function of the observation angle ϕ. **e**, Peak intensity of the ASE signal as a function of ϕ.
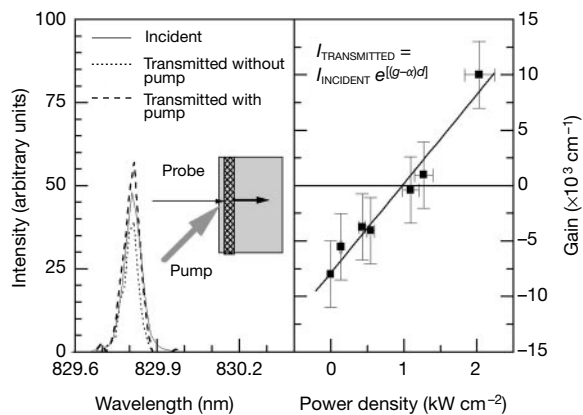
Figure 3 Spectral dependence of the net modal gain. Sample A, circles; sample B, triangles. The experimental conditions were as in Fig. 2. The large error bars result from both the low signal-to-noise ratio of the streak camera detection for low intensity signals and from the numerical procedure used for obtaining the modal gain from the ASE data[30,31].

low power density, we measured absorption; when the pump power was increased, the peak net modal gain increased and then saturated at values of about $100 \, \text{cm}^{-1}$ for power densities of about $5 \, \text{kW cm}^{-2}$.

By measuring the amplified signal for various wavelengths we obtained the gain spectrum for both samples A and B (Fig. 3; see also Supplementary Information). A wide spectral band is observed which spectrally overlaps the wavelength range of the luminescence, demonstrating that amplification is produced by the radiative state associated with the nanocrystal–oxide interface. We noticed that both samples yielded similar shapes and values for the gain curve. A confirmation of these findings was the observation of a strong emission lineshape narrowing (Fig. 4), either when the pump power density P is increased with fixed excitation length l (Fig. 4a), or when the excitation length l is increased with a fixed P (Fig. 4b). When l and P are fixed and the observation angle ϕ is changed (Fig. 4c–e), a significant intensity decrease and a broadening of the amplified emission spectrum occur as soon as there is deviation from the strict one-dimensional amplifier configuration, that is, when $\phi > 0°$. These observations support also the waveguide formation in our samples.

The most direct evidence of light amplification from our systems was provided by pump and probe transmission measurements. An intense laser beam (pump) at 390 nm excites the sample in order to reach the population inversion needed for amplification, while a weak probe signal at $\sim 800 \, \text{nm}$ passes through the active layer of thickness d. In the presence (absence) of the pump beam the probe beam is amplified (absorbed). In Fig. 5 we show the results. The probe signal is clearly amplified when passing through the excited nanocrystals. To our knowledge, this is the first evidence of light amplification in transmission, usually named single-pass gain, in Si-based systems. We deduced the net material gain values by using the formula given in Fig. 5; they are high enough to compare with those of self-assembled quantum dots made of III–V semiconductors[25,26]: $10,000 \pm 3,000 \, \text{cm}^{-1}$. This value has a very large error bar because of the geometry of the active nanocrystal layer and the losses in the quartz substrate. No change in probe intensity in the presence/absence of the pump beam was observed when the probe beam passed through pure quartz (without nanocrystals). Moreover, by decreasing the pump intensity (Fig. 5, right panel) we measured even absorption of the probe beam (population inversion is no

longer reached in nanocrystals). By changing the probe wavelength the net material gain decreased and eventually disappeared (amplification is lost when the probe energy is no longer in resonance with the transition for which population inversion is achieved) with an overall spectral dependence similar to that shown in Fig. 3 (see also Supplementary Information).

Gain cross-section per nanocrystal

By using the formalism of ref. 27 and the measured probe beam transmission under inversion conditions, we estimated a maximum-gain cross-section per nanocrystal $\gamma_T \approx 5 \times 10^{-16} \, \text{cm}^2$. It is interesting to compare this gain cross-section per nanocrystal with the photon absorption cross-section per nanocrystal (σ). We have hence directly measured the absorption cross-sections of ion-implanted Si nanocrystals by studying the rise time of the photoluminescence intensity as a function of pump power in a fashion similar to that recently reported for porous Si[28].
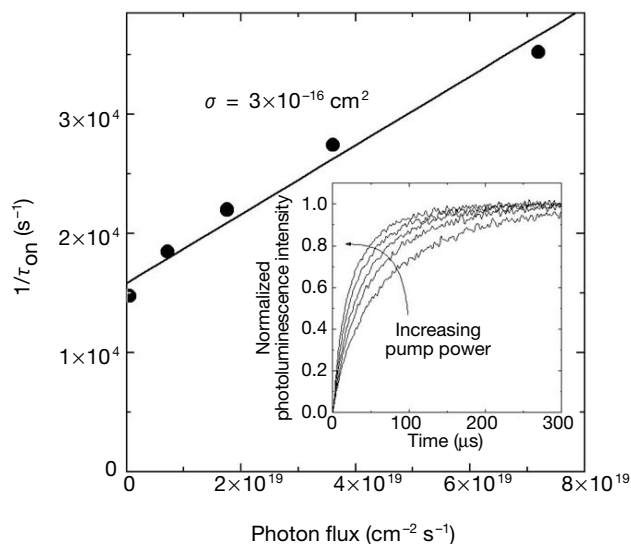
The photoluminescence intensity is given by $1 \propto N^*/\tau_R$, where N^* is the concentration of excited nanocrystals and τ_R the radiative lifetime. The rate equation for nanocrystal excitation will be:

$$\frac{\mathrm{d}N^\star}{\mathrm{d}t} = \sigma J(N - N^\star) - \frac{N^\star}{\tau} \qquad (2)$$

where J is the photon flux, N is the concentration of nanocrystals and τ is the decay time, taking into account both radiative and non-radiative processes. If a continuous wave (CW) pumping laser is turned on at $t = 0$, N^* will change according to equation (2) and the photoluminescence intensity will increase according to the following law:

$$I(t) = I_0\left\{1 - \exp\left[-\left(\sigma J + \frac{1}{\tau}\right)t\right]\right\} = I_0\left\{1 - \exp\left[-\left(\frac{t}{\tau_{\mathrm{on}}}\right)\right]\right\} \qquad (3)$$

A measure of the photoluminescence rise time as a function of J will therefore give direct information on the absorption cross-section. The inset to Fig. 6 shows $I(t)$ at 850 nm for Si nanocrystals pumped at 488 nm for different pump powers P. As predicted by equation (3), the photoluminescence rise time becomes shorter and shorter

Figure 5 Gain measurements. Left panel, spectrum of the transmitted probe beam measured in presence (dashed line) or in absence (dotted line) of the pump beam. The spectrum of the transmitted probe beam in absence of the absorbing\amplifying nanocrystal medium is also reported (continuous line) and named the incident beam. The inset shows the principle of the experiment. The formula used to deduce the material gain is also reported, d being the thickness of the active region. The probe beam was provided by a Kr lamp, which was imaged to a spot size of about $0.01 \, \text{mm}^2$ on the sample surface. The pump beam had a mean power of about $2 \, \text{kW cm}^{-2}$ and a wavelength of 390 nm. Right panel, dependence of the material gain value on the pump power density.

Figure 6 Reciprocal of the rise time τ_{on} as a function of the pump laser photon flux as obtained from a fit to the time resolved photoluminescence data shown in the inset. The slope gives the photon absorption cross-section σ. Inset: time resolved photoluminescence intensity at 850 nm switching on the 488 nm line of a CW Ar pumping laser at $t = 0$; data are taken at room temperature, at different pump powers (in the 0.8–80 mW range) and are normalized to the maximum intensity.

as P is increased. By fitting these curves with equation (3) we obtain the values of the rise time, τ_{on}, at the different P values. The reciprocal of τ_{on} is reported in Fig. 6 as a function of J. The data follow a straight line with a slope $\sigma \approx 3 \times 10^{-16}$ cm^2. The intercept of the fitted straight line with the vertical axis gives the lifetime of the Si nanocrystals in the system at the measured wavelength. The obtained value (70 µs) is in agreement with decay time measurements at 850 nm on the same sample. In this way we have been able to obtain a direct measurement of the photon absorption cross-section of the nanocrystals. Although this measurement is performed at an excitation wavelength of 488 nm, it should reflect the property of the 800 nm state because absorbance at these two wavelengths is identical (see Fig. 1). We note that, as theoretically predicted[15], the measured absorption cross-section σ is of the same order of magnitude as the gain cross-section γ_T. The same agreement is found when we compare the net material gain to the absorption coefficient deduced by the absorbance data of Fig. 1.

Another important issue concerns the comparison of the gain cross-sections that are derived from the modal and the material gain. It was shown in ref. 27 that in the variable stripe-length geometry, the gain cross-section per nanocrystal (γ_{ASE}) can be derived by using

$$\gamma_{ASE} = \frac{g}{(f_c - f_v)N\Gamma} \qquad (4)$$

where Γ is the optical filling factor of the amplified mode. By assuming a complete population inversion $f_c - f_v = 1$, an optical filling factor of 0.097 and the measured net modal gain $g \approx 100$ cm^{-1}, one finds $\gamma_{ASE} \approx 5 \times 10^{-17}$ cm^2. This is a lower limit to γ_{ASE}. If we consider an incomplete inversion or a weaker confining waveguide (that is, no step index profile in the waveguide and/or a lower effective refractive index for the nanocrystal), γ_{ASE} will significantly increase. For example, by using the Γ value computed for the refractive index measured in PE-CVD nanocrystals[17], we obtain $\gamma_{ASE} \approx 3 \times 10^{-16}$ cm^2. The difference between the two estimated values of γ_{ASE} may be an indication of the quantitative uncertainty on the gain cross-section values determined by the gain measurements.

A comparison of the gain cross-sections per nanocrystal derived by transmission (γ_T) and by the variable strip length method (γ_{ASE}) shows that the two values are in reasonable quantitative agreement. Indeed, the determined value of γ_{ASE} is only a lower limit and there

are large error bars on the pump and probe determined gain coefficients.

Origin of gain

The wide spectral gain of inhomogeneous nature is energetically matching both the luminescence emission and the 800-nm interface state absorption band. For these reasons, a three-level model is proposed to explain the observed gain (Fig. 7): two levels correspond to the lowest unoccupied molecular orbital (LUMO), or the bottom of the conduction band, and to the highest occupied molecular orbital (HOMO), or the top of the valence band of the nanocrystal, respectively. The third level is due to the radiative interface state observed in absorption and responsible for the luminescence emission band at 800 nm. Optical excitation populates the LUMO, emptying the HOMO. Electrons from the LUMO relax very rapidly to the interface state. Electrons in the interface state have long lifetimes. Indeed, the absorption band at 800 nm, the Stokes shift between absorption and luminescence, the fast rise and the slow decay times of the 800-nm luminescence under picosecond excitation, and the efficient luminescence emission of the 800-nm luminescence all support this energy model. Within the model, the rate of depopulation of the initial state is much faster than its filling rate via a carrier recombination mediated by the interface state. Population inversion between the HOMO and the radiative state associated with the nanocrystal–oxide interface is thus possible. This model also explains why losses due to free carrier absorption that usually exceed the gain by stimulated emission in other Si based systems[29], or those due to Auger recombinations[22], are not effective here. In addition, model calculations[10] show that the size dependence of the radiative interface state energy is smaller than that of conduction-to-valence band transitions, relaxing issues related to the broad distribution of sizes.

Using the measured absorption cross-section σ per nanocrystal, we estimate that under our peak excitation condition of about 10^{22} photons cm^{-2} s^{-1}, more than 100 electron–hole pairs per nanocrystal are generated. As we have nanocrystals with about 500 Si atoms, of which about 35% are surface atoms, we have about 150 interface states available per Si nanocrystal when we assume that each surface Si atom is bound to an O atom. In Fig. 5, we show that to have optical gain the excitation level should be high enough to invert most of these states.

In Table 1 we report a compilation of data on the gain cross-section per quantum dot for some III–V semiconductors. It can be noticed that the silicon nanocrystal values are about three orders of magnitude lower than the one typically found in InAs quantum dots. We argue that this is due to the indirect bandgap of Si and to the fact that the gain is due to radiative interface states. Despite this difference, the net material gain is of the same order of magnitude between Si nanocrystals and InAs quantum dot systems, owing to the much higher areal density of nanocrystals that is achievable with the ion-implantation method used in this work. We note that the gain cross-section per nanocrystal γ is inversely proportional to the radiative lifetime τ_R (ref. 15). By looking at the γ data in Table 1, we infer large differences in lifetimes. Indeed radiative lifetimes in the microsecond range are measured for Si nanocrystals, whereas for InAs quantum dot lifetimes in the nanosecond range were reported[25,26].
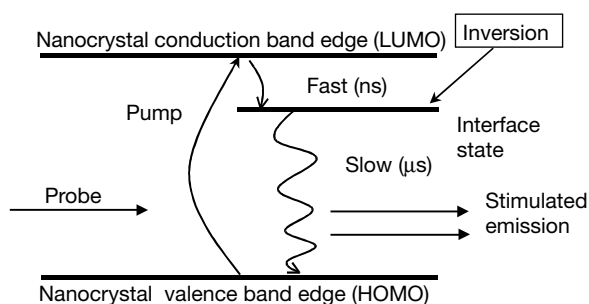
Figure 7 Schematic energy diagram for a nanocrystal showing how population inversion can be reached in this system.

Table 1 Gain cross-section per quantum dot or nanocrystal

Quantum dot material	Net model gain (cm^{-1})	Net material gain ($\times 10^4$ cm^{-1})	Areal dot density (cm^{-2})	Active layer thickness (nm)	Filling factor (10^{-4})	Gain cross-section per dot (10^{-16} cm^2)	Reference
InAs single layer quantum dot	8.2	9*	1×10^{11}	1.7	1.2	1,200	25
InAs 7 stacks quantum dot	70–85	1.5*	1×10^{11}	100	48	4,000	26
GaAs single layer quantum dot	13*		1×10^{10}			450*	27
Si nanocrystals	100	1	2×10^{14}	100	970	0.5–5	This work

*Calculated approximately.

Conclusions

Modal and net material optical gains have been observed unambiguously in Si nanocrystals. Quantitative estimates of gain cross-section per nanocrystal show that the measured values are orders of magnitude lower than those found in III–V semiconductor quantum dots. However, owing to the much higher stacking density of Si nanocrystals with respect to direct-bandgap quantum dots, similar values for the material gain are observed. These findings open a route towards the realization of a silicon-based laser. □

1. Canham, L. T. Silicon quantum wire array fabrication by electrochemical and chemical dissolution of wafers. *Appl. Phys. Lett.* **57,** 1045–1048 (1990).
2. Cullis, A. G. & Canham, L. T. Visible light emission due to quantum size effects in highly porous crystalline silicon. *Nature* **353,** 335–338 (1991).
3. Wilson, W. L., Szajowski, P. F. & Brus, L. E. Quantum confinement in size-selected surface-oxidised silicon nanocrystals. *Science* **262,** 1242–1244 (1993).
4. Lu, Z. H., Lockwood, D. J. & Baribeau, J.-M. Quantum confinement and light emission in SiO₂/Si superlattices. *Nature* **378,** 258–260 (1995).
5. Hirschman, K. D., Tsybeskov, L., Duttagupta, S. P. & Fauchet, P. M. Silicon-based light emitting devices integrated into microelectronic circuits. *Nature* **384,** 338–340 (1996).
6. Franzò, G., Priolo, F., Coffa, S., Polman, A. & Carnera, A. Room temperature electroluminescence from Er doped crystalline silicon. *Appl. Phys. Lett.* **64,** 2235–2237 (1994).
7. Leong, D., Harry, M., Reeson, K. J. & Homewood, K. P. A silicon/iron disilicide light-emitting diode operating at a wavelength of 1.5 μm. *Nature* **387,** 686–688 (1997).
8. Nassiopoulos, A. G., Grigoropoulos, S. & Papadimitriou, D. Electroluminescent device based on silicon nanopillars. *Appl. Phys. Lett.* **69,** 2267–2269 (1996).
9. Bisi, O., Ossicini, S. & Pavesi, L. Porous silicon: a quantum sponge structure for silicon based optoelectronics. *Surf. Sci. Rep.* **38,** 1–126 (2000).
10. Wolkin, M. V., Jorne, J., Fauchet, P. M., Allan, G. & Delerue, C. Electronic states and luminescence in porous silicon quantum dots: the role of oxygen. *Phys. Rev. Lett.* **82,** 197–200 (1999).
11. Miller, D. A. Silicon sees the light. *Nature* **378,** 238 (1995).
12. Iyer, S. S. & Xie, Y.-H. Light emission from silicon. *Science* **260,** 40–46 (1993).
13. Silicon based optoelectronics. *Mater. Res. Bull.* **23(4),** (1998).
14. Fauchet, P. M. The integration of nanoscale porous silicon light emitters: materials science, properties and integration with electronic circuitry. *J. Lumin.* **80,** 53–64 (1999).
15. Yariv, A. *Quantum Electronics* 2nd edn (Wiley & Sons, New York, 1974).
16. Canham, L. T. in *Frontiers of Nano-Optoelectronic Systems* (eds Pavesi, L. & Buzaneva, E.) 85–98 (Kluwer Academic, Dordrecht, 2000).
17. Iacona, F., Franzò, G. & Spinella, C. Correlation between luminescence and structural properties of Si nanocrystals. *J. Appl. Phys.* **87,** 1295–1303 (2000).
18. Kovalev, D., Heckler, H., Polisski, G. & Koch, F. Optical properties of Si nanocrystals. *Phys. Status Solidi* **251,** 871–930 (1999).
19. Kanemitsu, Y. & Okamoto, S. Quantum confinement and interface effects on photoluminescence from silicon single quantum wells. *Solid State Commun.* **103,** 573–576 (1997).
20. Kanemitsu, Y. & Okamoto, S. Phonon structures and Stokes shift in resonantly excited luminescence of silicon nanocrystals. *Phys. Rev. B* **58,** 9652–9655 (1998).
21. Degoli, E. & Ossicini, S. Quantum confined and interface states related visible luminescence in Si/SiO₂ superlattices. *Surf. Sci.* (in the press).
22. Klimov, V. I., Schwarz, Ch., McBranch, D. W. & White, C. W. Initial carrier relaxation dynamics in ion-implanted Si nanocrystals: femtosecond transient absorption study. *Appl. Phys. Lett.* **73,** 2603–2605 (1998).
23. Linnros, J., Galeckas, A., Lalic, N. & Grivickas, V. Time-resolved photoluminescence characterisation of nm-sized silicon nanocrystallites in SiO₂. *Thin Solid Films* **297,** 167–170 (1997).
24. Shaklee, K. L., Nahaory, R. E. & Leheny, R. F. Optical gain in semiconductors. *J. Lumin.* **7,** 284–309 (1973).
25. Kirstaedter, N. *et al.* Gain and differential gain of single layer InAs/GaAs quantum dot injection lasers. *Appl. Phys. Lett.* **69,** 1226–1228 (1996).
26. Lingk, C. *et al.* Dynamics of amplified spontaneous emission in InAs/GaAs quantum dots. *Appl. Phys. Lett.* **76,** 3507–3509 (2000).
27. Blood, P. On the dimensionality of optical absorption, gain and recombination in quantum-confined structures. *IEEE J. Quantum Electron.* **36,** 354–362 (2000).
28. Kovalev, D. *et al.* Optical absorption cross sections of Si nanocrystals. *Phys. Rev. B* **61,** 4485–4487 (2000).
29. von Behren, J., Kostoulas, Y., Ucer, K. B. & Fauchet, P. M. The femtosecond optical response of porous, amorphous and crystalline silicon. *J. Non-Cryst. Solids* **198–200,** 957–960 (1996).
30. Jordan, V. Gain measurements of semiconductor laser diodes: requirements for wavelength resolution and sensitivity to noise. *IEE Proc. Optoelectron.* **141,** 13–15 (1994).
31. Hvam, J. M. Direct recording of optical gain spectra from ZnO. *J. Appl. Phys.* **49,** 3124–3126 (1978).